Catal Lett (2014) 144:905–911
DOI 10.1007/s10562-014-1235-3

Effect of Pd Particle Size on the Direct Synthesis of Hydrogen Peroxide from Hydrogen and Oxygen over Pd Core–Porous SiO_2 Shell Catalysts

Seongmin Kim · Dae-Won Lee · Kwan-Young Lee · Eun Ae Cho

Received: 3 December 2013 / Accepted: 4 March 2014 / Published online: 23 March 2014

Abstract The catalytic activity of Pd core–porous SiO_2 shell catalysts (Pd@SiO_2) with different Pd particle size was evaluated for the direct synthesis of hydrogen peroxide from hydrogen and oxygen. In the synthesis of palladium nanoparticles, the Pd particle size increased with the decrease of the ratio of polyvinylpyrrolidone (PVP) to Pd. Among the prepared Pd@SiO_2 catalysts, Pd@SiO_2_PVP2 (Pd loading = 1.02 wt%; PVP to Pd precursor molar ratio = 2) had the largest Pd particle size (4.2 nm) and showed the highest hydrogen peroxide production rate (330 mmol H_2O_2/g_{Pd}·h). The production rate of hydrogen peroxide decreased along with the decrease in Pd particle size. As the Pd nanoparticles became smaller, energetic sites (defects, edges, and corners) where the O–O bond is dissociated and the formation of water is promoted were more exposed on the surface. Thus, fewer energetic sites on the Pd surface are favored for synthesizing hydrogen peroxide, which was the major reason for Pd@SiO_2_PVP2 being the most active among the prepared Pd@SiO_2 catalysts.

S. Kim · D.-W. Lee (✉) · K.-Y. Lee (✉)
Department of Chemical and Biological Engineering, Korea University, 145 Anam-ro, Seoul 136-713, Republic of Korea
e-mail: stayheavy@korea.ac.kr

K.-Y. Lee
e-mail: kylee@korea.ac.kr

K.-Y. Lee
Green School, Korea University, 145 Anam-ro, Seoul 136-713, Republic of Korea

E. A. Cho
Fuel Cell Research Center, Korea Institute of Science and Technology, Hawolgok-dong, Sungbuk-gu, Seoul, Republic of Korea

Keywords Direct hydrogen peroxide synthesis · Palladium catalyst · Core–shell structured catalyst · Palladium nanoparticle · Colloidal method

1 Introduction

Hydrogen peroxide is a chemical widely used in industrial applications such as pulp and textile bleaching, waste water treatment, and semiconductor cleaning [1]. Also, it is applied as an oxidant for high-value partial oxidation reactions such as benzene to phenol [2] and propylene to propylene oxide [3]. Hydrogen peroxide is a clean and efficient oxidant with 47 wt% O_2 per molecule, which is the highest among commercial oxidants (for example, HNO_3, which is the oxidant for adipic acid synthesis, has 25 wt% O_2 per molecule). Moreover, it is converted to water after reaction and does not produce any byproduct of environmental concern.

Hydrogen peroxide is commercially produced by the anthraquinone auto-oxidation process (AO process). The AO process is composed of sequential hydrogenation and oxidation of anthraquinone and is economically viable for large-scale production (4–6 tons/year) [4]. However, the AO process not only generates environmentally harmful wastes, but also consumes a significant amount of energy [5]. An alternative process is the direct synthesis of hydrogen peroxide from hydrogen and oxygen (Fig. 1), which uses little or no organic solvents and consumes less energy [1].

However, the direct hydrogen peroxide synthesis usually results in a low hydrogen peroxide production rate because of difficulties in controlling undesired water-forming reactions such as direct synthesis of water (Route II in Fig. 1) and hydrogenation (Route III in Fig. 1) or decomposition (Route

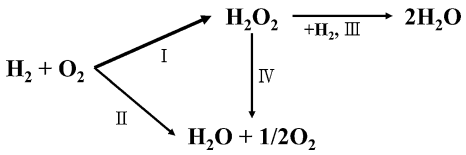

Fig. 1 The reactions involved in the direct synthesis of hydrogen peroxide from hydrogen and oxygen

IV in Fig. 1) of synthesized hydrogen peroxide (into water). To suppress the undesired side reactions (water-forming reactions), acids and halide ions are introduced to the reaction media [6, 7], or acidic support materials are applied to the catalysts [8, 9].

Pd-supported catalysts have been mostly used in studies on direct hydrogen peroxide synthesis. The reaction additives (acids and halides) are used to elevate the activity of a catalyst, but the physicochemical state of Pd plays a pivotal role in determining the production rate of hydrogen peroxide. For example, alloying Pd with Au or Pt enhances hydrogen peroxide selectivity, and it has been proven that the enhancement effect of alloying is based on the modification of the physical or electronic state of Pd [10, 11]. It is known that energetic sites such as defects, corners, and edges on the Pd surface promote water formation and are undesirable for the hydrogen peroxide selectivity [12]. It has also been suggested that the Pd (110) plane has a more proper atomic configuration for synthesizing hydrogen peroxide than those of the (100) and (111) planes [13].

Recently, fcc noble metals (Pt, Pd, and Au) have been synthesized at the nano scale with uniform size and shape using the colloidal method [14, 15]. The morphology-controlled nanoparticles are applied as catalysts for various gas-phase, liquid-phase, or electrocatalytic reactions, most of which showed good activities by increasing the surface-to-volume ratio or exposing a specific facet favored in the reaction [16–18]. The nanoparticles can be used directly as a catalyst, but recovering colloid nanoparticles is inconvenient (especially in liquid-phase reactions), which is not desirable if considering a commercial catalytic process. In our previous work, Pd nanoparticles with uniform size were synthesized, which showed an enhanced activity for the direct synthesis of hydrogen peroxide compared to conventional impregnated Pd particles [19]. Moreover, the recovery problem was solved by encapsulating Pd nanoparticles inside silica shells by applying a Pd core–porous SiO_2 shell structure.

We have since extended that study to examine the influences of the size of Pd nanoparticles on the direct hydrogen peroxide synthesis activity of Pd core–porous SiO_2 shell catalysts. The Pd nanoparticles could be synthesized with different particle size by varying the ratio of polyvinylpyrrolidone (PVP) to Pd precursors in a colloidal preparation method. In this study, we investigated the influences of the PVP-to-Pd precursor ratio on the dimension of Pd nanoparticles and textural properties of entire catalysts, and tried to find their relationships to the activity of the catalyst.

2 Experimental

2.1 Catalyst Preparation

The synthesis of Pd core–porous SiO_2 shell catalyst was composed of two steps: (1) the synthesis of colloidal Pd nanoparticles and (2) the encapsulation of Pd nanoparticles in silica. Palladium nanoparticles were synthesized by a colloidal method. First, 0.141 g of $Pd(NO_3)_2{\cdot}H_2O$ (Sigma-Aldrich) and a specific amount of PVP (MW: 55000; Sigma-Aldrich) were dissolved in 12 mL of deionized water (DI water). The amount of PVP was determined to meet the PVP-to-Pd precursor weight ratio (0, 2, 4, or 8). A 150-μL aliquot of formaldehyde (37 wt% in H_2O, Sigma-Aldrich) and 0.04 g of sodium hydroxide (Sigma-Aldrich) were introduced to the prepared solution. Then, the mixture was stirred for 2 h at room temperature. The formation of Pd nanoparticles was confirmed by a color change from brown to dark black. Acetone was added to the slurry, which was centrifuged at 13,000 rpm for 10 min to separate the PVP-stabilized Pd particle slurry from the aqueous solution. The prepared Pd nanoparticle slurry was denoted as "Pd_PVPX," where X implies the weight ratio of PVP to Pd precursor (X = 0, 2, 4, or 8).

The Stöber method was introduced to immobilize the Pd nanoparticles inside porous silica [19]. The PVP-stabilized Pd nanoparticle slurry was re-dispersed in 200 mL of ethanol. 18 mL of DI water, 10 mL of NH_4OH (37–39 wt% in H_2O, Sigma-Aldrich), and 20 mL of tetraethyl orthosilicate (TEOS; Sigma-Aldrich) were added one by one, and the solution was stirred for 24 h at room temperature. The Pd-encapsulated silica was filtered and washed with ethanol several times. The filtered cake was dried overnight at 60 °C in a vacuum. Prepared catalysts were then calcined at 500 °C for 3 h and reduced by 10 vol% H_2/N_2 gas at 350 °C for 1 h. The catalysts were denoted as "Pd@SiO_2_PVPX," implying that Pd_PVPX is encapsulated by silica.

2.2 Catalyst Characterization

The morphology and size of catalysts were examined by transmission electron microscopy (TEM: Tecnai F20, FEI). The crystalline structure was analyzed by X-ray diffraction (XRD: D/MAX-2500/PC, Rigaku). The specific surface area and pore volume were calculated from N_2 physisorption (at

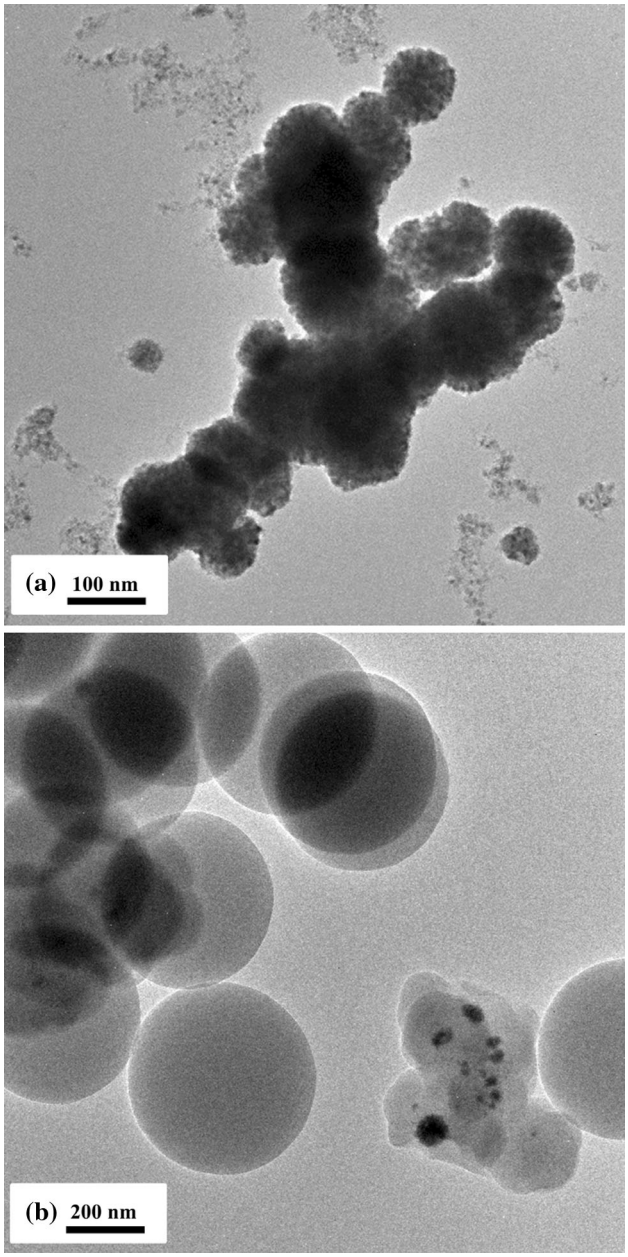

Fig. 2 TEM images of **a** Pd synthesized *without* PVP (i.e., Pd_PVP0) and **b** Pd@SiO_2_PVP0

77 K) data obtained from a BET instrument (ASAP2010, Micromeritics). The Pd content was measured by inductively coupled plasma atomic emission spectroscopy (ICP-AES: JY Ultima2C, Jobin–Yvon). The metal surface area was measured by CO chemisorption (ASAP 2010, Micromeritics).

2.3 Reaction Test

The catalytic reaction for the direct synthesis of hydrogen peroxide from hydrogen and oxygen was performed in a double jacket glass reactor. The reaction tests were carried out at 20 °C and atmospheric pressure for 3 h while agitating the reactor at 1,200 rpm. The catalyst loading was 0.2 g. A 150-mL amount of solution (20 vol% ethanol in DI water) was used as the reaction medium. Potassium bromide (0.9 mM) and phosphoric acid (0.03 M) were added to suppress the conversion of the hydrogen peroxide. The total flow rate of gaseous reactants was 22 mL/min, and the hydrogen-to-oxygen ratio was 1/10. The hydrogen peroxide concentration was measured through iodometric titration [19], and the hydrogen concentration was measured with gas chromatography for calculating the hydrogen conversion (Younglin, ACME6000).

3 Results and Discussion

3.1 Characterization of Pd Nanoparticle and Pd Core–Porous SiO_2 Shell Catalyst

TEM images of the Pd nanoparticles synthesized *without* PVP (i.e., Pd_PVP0) and Pd_PVP0 immobilized in silica (i.e., Pd@SiO_2_PVP0) are shown in Fig. 2. Figure 2a shows that the Pd particles in Pd_PVP0 were severely aggregated. The attempt to encapsulate the Pd particles inside silica was not successful. It was found that most of the silica spheres were formed extraneously from the Pd particles (Fig. 2b).

TEM images of the Pd particles synthesized *with* PVP (Pd_PVP2, 4, and 8) are presented in Fig. 3, each of which was paired with the corresponding size distribution of Pd particles. Compared to Pd_PVP0, the Pd_PVP2, 4, and 8 consisted of nano-scale Pd particles, and the shapes of particles were uniform. As the PVP-to-Pd precursor ratio increased from 2 to 8, the average Pd particle size decreased from 4.1 to 3.5 nm. It is known that the carbonyl groups of PVP coordinates to the Pd atoms and influences the growth rate of Pd particles [20]. Yan et al. made a similar claim about the synthesis of Ru nanoparticles that the PVP protects and stabilizes the Ru colloids, and an increase of the PVP/Ru ratio resulted in smaller Ru nanoparticles [21].

The prepared PVP-stabilized Pd nanoparticle slurry was encapsulated with silica using the Stöber method. Then, pores were formed over the silica shell with combusting PVP molecules through calcination, and the final form of the catalyst was obtained after hydrogenation, through which the Pd particles that had been oxidized during calcination were reduced back to their metallic states. TEM images of the encapsulated Pd catalysts (Pd@SiO_2_PVP2, 4, and 8) are presented in Fig. 4, which shows well-formed Pd core–SiO_2 shell structures. The mean size of Pd particles entrapped in the silica shell was measured from the

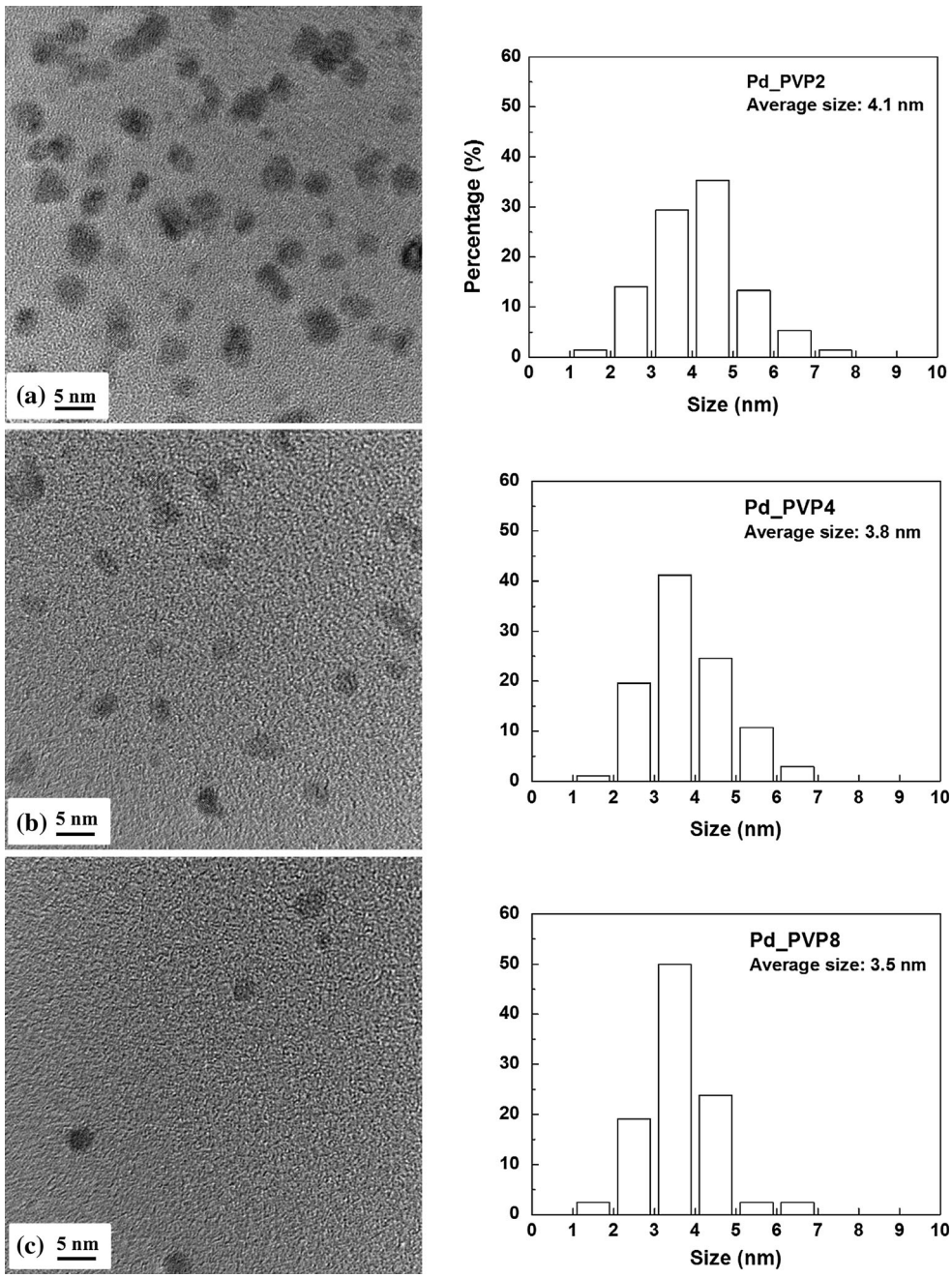

Fig. 3 TEM images and particle size distribution of Pd nanoparticles: **a** Pd_PVP2, **b** Pd_PVP4, and **c** Pd_PVP8

TEM images, and the results are listed in Table 1. Even though the catalysts experienced a series of high-temperature treatments (calcination and reduction), the dimension of pristine Pd particles (4.1, 3.8, and 3.5 nm, in Fig. 3) was well retained. It was supposed that the silica shell acted as a barrier to the migration and agglomeration of Pd particles during high-temperature treatments.

The textural properties of Pd@SiO_2_PVP2, 4, and 8 are summarized in Table 2. Pd@SiO_2_PVP2, 4, and 8 showed well-developed micro- and meso-size pore structures. The increase in the PVP-to-Pd precursor ratio led to a higher BET surface area and pore volume. In contrast, Pd@SiO_2_PVP0 was almost non-porous (not shown here) because it was synthesized in the absence of PVP.

XRD patterns of Pd@SiO_2 catalysts are presented in Fig. 5. Pd@SiO_2_PVP0 showed only a broad diffraction pattern of silica ($2\theta = 21°$, JCPDS #862364), and none of the Pd-related signal was detected, because most of the Pd particles, which we had failed to encapsulate with silica shells, were lost during the washing procedure. The XRD patterns of Pd@SiO_2_PVP4 and PVP8 did not include a Pd peak either, but it might be due to the nano-size of Pd

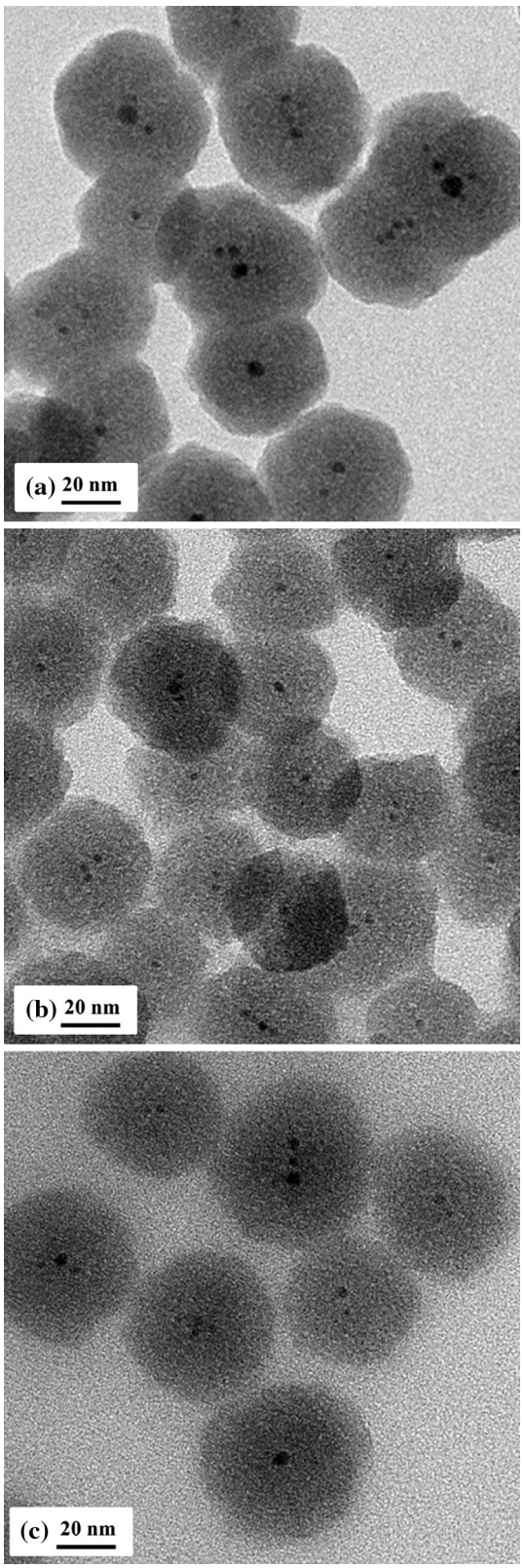

Fig. 4 TEM images of $Pd@SiO_2$ after calcination and reduction: **a** $Pd@SiO_2$_PVP2, **b** $Pd@SiO_2$_PVP4, and **c** $Pd@SiO_2$_PVP8

Table 1 Particle size of Pd nanoparticles in $Pd@SiO_2$

Catalyst	Mean particle size (nm)	SD (nm)
$Pd@SiO_2$_PVP2	4.2	1.5
$Pd@SiO_2$_PVP4	3.7	1.5
$Pd@SiO_2$_PVP8	3.4	1.1

Table 2 Textural properties (BET surface area and pore properties) of $Pd@SiO_2$

Catalyst	BET surface area (m^2/g)	Micropore surface area[a] (m^2/g)	Mesopore Volume[b] (cm^3/g)	Micropore volume[a] (cm^3/g)
$Pd@SiO_2$_PVP2	169	108	0.099	0.042
$Pd@SiO_2$_PVP4	320	205	0.351	0.082
$Pd@SiO_2$_PVP8	323	211	0.402	0.086

[a] Obtained using t-plot method

[b] Obtained using BJH desorption cumulative pore volume analysis

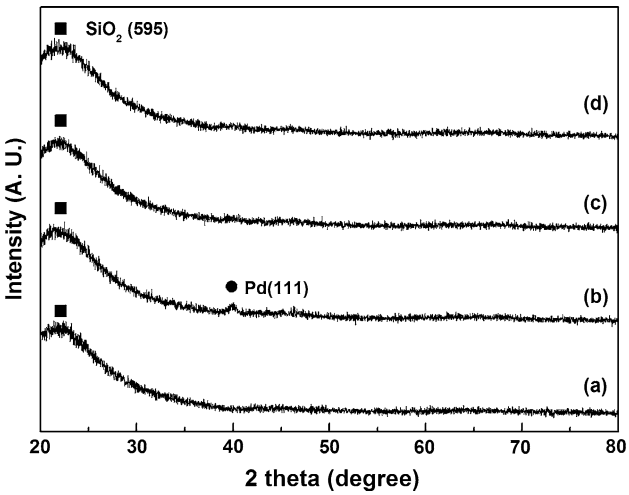

Fig. 5 XRD patterns of $Pd@SiO_2$ after calcination and reduction: *a* $Pd@SiO_2$_PVP0, *b* $Pd@SiO_2$_PVP2, *c* $Pd@SiO_2$_PVP4 and *d* $Pd@SiO_2$_PVP8

particles and their high dispersion over the silica shell. Meanwhile, $Pd@SiO_2$_PVP2, which had a bigger particle size than $Pd@SiO_2$_PVP4 and PVP8, showed a slight peak at $2\theta = 39°$, which corresponded to the typical (111) peak of an fcc Pd metal (JCPDS #870645).

The Pd loading and metal dispersion of the $Pd@SiO_2$ catalysts are presented in Table 3. For all the samples, the Pd loading was close to the theoretical value of 1 wt%. The metallic surface areas of $Pd@SiO_2$_PVP2 and $Pd@SiO_2$_PVP4 were approximately 60 m^2/g. $Pd@SiO_2$_PVP8

Table 3 Pd loading and (exposed) Pd surface area of $Pd@SiO_2$

Catalyst	Pd loading (wt%)	Pd surface area (m^2/g)
$Pd@SiO_2$_PVP2	1.02	62
$Pd@SiO_2$_PVP4	0.98	60
$Pd@SiO_2$_PVP8	0.88	76

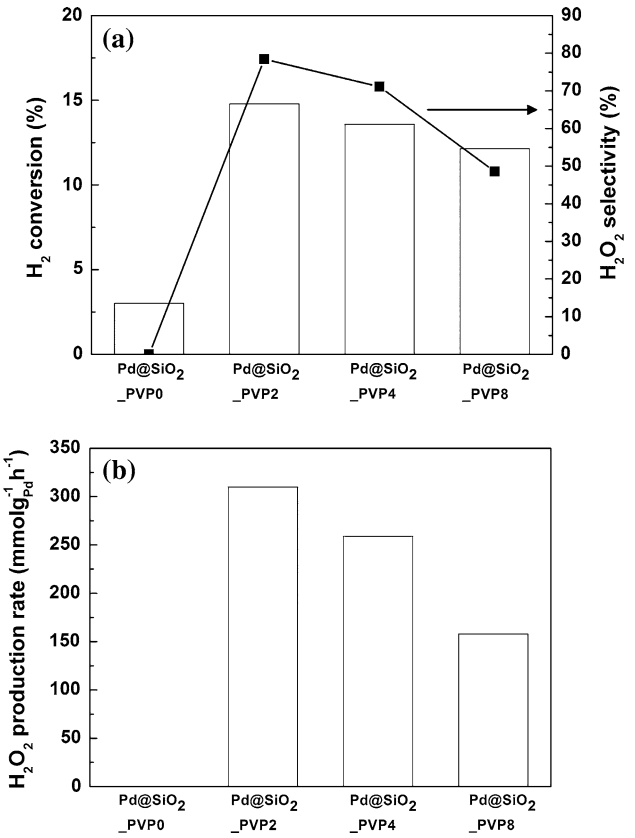

Fig. 6 Catalytic activity of $Pd@SiO_2$_PVP*X* ($X = 0$, 2, 4, and 8) in the direct synthesis of hydrogen peroxide: **a** hydrogen conversion and hydrogen peroxide selectivity, **b** production rate of hydrogen peroxide

showed a slightly high value (76 m^2/g), as it contained Pd particles which were smaller than those of the prior two samples.

3.2 Activity Test for Direct Synthesis of Hydrogen Peroxide

The activity test results of $Pd@SiO_2$ are presented in Fig. 6. $Pd@SiO_2$_PVP0 showed very low hydrogen conversion (less than 3 %) and an undetectably low production rate of hydrogen peroxide, which might be mainly due to the deficiency of Pd particles and the non-porous silica structure. The hydrogen conversion of $Pd@SiO_2$_PVP2, PVP4, and PVP8 was much higher (12, 13, and 14 %, respectively) than that of $Pd@SiO_2$_PVP0. It implies that the pores formed via the thermal decomposition of PVP functioned as paths for diffusion of the reactants and products between the pore entrance and Pd particle surface. However, the hydrogen conversion, hydrogen peroxide selectivity, and production rate decreased with the increase of the PVP-to-Pd precursor ratio, (i.e., the increase of BET area and total pore volume), implying that there was no significant correlation between the textural properties and activity. Interestingly, $Pd@SiO_2$_PVP2, which had the lowest BET surface area and pore volume and the largest mean Pd particle size, showed the highest hydrogen peroxide production rate of 310 $mmol/g_{Pd}{\cdot}h$. It also had the highest hydrogen conversion (14.8 %) and hydrogen peroxide selectivity (78.4 %).

To obtain high hydrogen peroxide selectivity, the proper control of O–O bond cleavage is important. The cleavages of O–O bonds in molecular oxygen and hydrogen peroxide are elementary steps that lead to the formation of water, which reduces the hydrogen peroxide selectivity and yield [10, 22].

It is well known that the structure of a metal surface determines the degree of dissociation of adsorbed molecules [23, 24]. Deguchi and Iwamoto performed a density-functional theory (DFT) study of direct hydrogen peroxide synthesis on a Pd surface, and claimed that the formation of water and decomposition of hydrogen peroxide would be preferred on coordinatively unsaturated sites such as corners and edges [25]. Menegazzo et al. and Ghedini et al. similarly claimed that the dissociation of molecular oxygen and water formation are favored on the defects, corners, and edges on a Pd surface [12, 26], and such energetic sites become abundant as the mean particle size of Pd decreases [27]. Therefore, it was supposed that the decrease of the H_2O_2 production rate with the increase of the PVP-to-Pd precursor ratio could be related to the decrease of the Pd particle size, which would promote O–O bond cleavages in oxygen and hydrogen peroxide, leading to by-product (water) formation.

4 Conclusion

Pd core–porous SiO_2 shell catalysts with different sizes of Pd nanoparticles were synthesized using colloidal nanoparticle synthesis and Stöber encapsulation methods. The mean Pd particle size decreased with the increase of the PVP-to-Pd precursor ratio. PVP-stabilized Pd particles were well encapsulated by silica shells, and the Pd particle sizes of the core–shell catalysts were similar to those of pristine Pd particles, even though the catalysts had experienced high-temperature thermal treatments. In activity tests, the production rate of hydrogen peroxide increased with the Pd particle size, so $Pd@SiO_2$_PVP2, which had

the largest Pd particles, showed the highest production rate among the tested catalysts. It was supposed that the highest activity of Pd@SiO_2_PVP2 is related to its smallest number of surface energetic sites (defects, corners, and edges), where by-product (water) formation was promoted via O–O bond cleavage reactions.

Acknowledgments This work was supported by the Human Resources Development program (No. 20114010203050) of the Korea Institute of Energy Technology Evaluation and Planning (KETEP) grant funded by the Korean government Ministry of Trade, Industry and Energy. This work was supported by the National Research Foundation of Korea Grant funded by the Korean Government (Ministry of Science, ICT & Future Planning)" (2013, University-Institute Cooperation Program). Dr. Dae-Won Lee was supported by a Korea University Grant.

References

1. Campos-Martin JM, Blanco-Brieva G, Fierro JLG (2006) Angew Chem Int Ed Engl 45(42):6962–6984
2. Zhang J, Tang Y, Li G, Hu C (2005) Appl Catal A 278:251–261
3. Laufer W, Meiers R, Holderich W (1999) J Mol Catal A 141:215–221
4. Mizuno N (2009) Modern heterogeneous oxidation catalysis. Wiley-VCH, Weinheim
5. Samanta C (2008) Appl Catal A 350:133–149
6. Choudhary VR, Gaikwad AG (2003) React Kinet Catal Lett 80:27–32
7. Ntainjua NE, Piccinini M, Pritchard JC, Edwards JK, Carley AF, Moulijn JA, Hutchings GJ (2009) ChemSusChem 2:575–580
8. Park S, Seo JG, Jung JC, Baeck SH, Kim TJ, Chung YM, Oh SH, Song IK (2009) Catal Commun 10:1762
9. Park S, Baeck SH, Kim TJ, Chung YM, Oh SH, Song IK (2010) J Mol Catal A 319:98–107
10. Edwards JK, Solsona B, Ntainjua E, Carley AF, Herzing AA, Kiely CJ, Hutchings GJ (2009) Science 323:1037–1041
11. Liu Q, Bauer JC, Schaak RE, Lunsford JH (2008) Appl Catal A 339:130–136
12. Ghedini E, Menegazzo F, Signoretto M, Mansoli M, Pinna F, Strukul G (2010) J Catal 273:266–273
13. Zhou B, Lee L-K, US Patent 6,168, 775
14. Xia Y, Xiong Y, Lim B, Skrabalak SE (2009) Angew Chem Int Ed Engl 48:60–103
15. Lim B, Jiang M, Tao J, Camargo PHC, Zhu Y, Xia Y (2009) Adv Funct Mater 19:189–200
16. Jin M, Liu H, Zhang H, Xie Z, Liu J, Xia Y (2011) Nano Res 4:83–91
17. Lee H, Kim C, Yang S, Han JW, Kim J (2012) Catal Surv Asia 16:14
18. Miyake M, Miyabayashi K (2012) Catal Surv Asia 16:1–13
19. Lee H, Kim S, Lee D-W, Lee K-Y (2011) Catal Commun 12:968
20. Teranishi T, Miyake M (1998) Chem Mater 10:594–600
21. Yan X, Liu H, Liew Y (2001) J Mater Chem 11:3387–3391
22. Piccinini M, Ntainjua E, Edwards JK, Carley AF, Mouljin JA, Hutchings GJ (2010) Phys Chem Chem Phys 12:2488–2492
23. Matsushima T (1989) Surf Sci 217:155
24. Rar A, Matsushima T (1994) Surf Sci 318:89–96
25. Deguchi T, Iwamoto M (2013) J Phys Chem C 117:18540
26. Menegazzo F, Signoretto M, Frison G, Pinna F, Strukul G, Manzoli M, Boccuzzi F (2012) J Catal 290:143–150
27. Hardeveld RV, Hartog F (1969) Surf Sci 15:189–230